


Article

# Design of All-Solid Dual-Concentric-Core Microstructure Fiber for Ultra-Broadband Dispersion Compensation

Chao Wang \*, Yajing Zhang, Zheng Wu, Guoxu Zhang, Yiyang Zhang and Linghong Jiang

Intelligence and Information Engineering College, Tangshan University, Tangshan 063000, China

\* Correspondence: wangchao\_198504@sina.com; Tel.: +86-155-1204-8666

Received: 16 July 2019; Accepted: 9 August 2019; Published: 15 August 2019



**Abstract:** In this paper, the all-solid dual-concentric-core microstructure fiber (MSF) with ultra-broadband dispersion compensation characteristics is designed. The effects of microstructure fiber structure parameters on dispersion, phase-matching wavelength, and kappa value are analyzed by the multi-pole method and mode coupling theory. The average dispersion compensation multiple is 18.45, that is, 1 km long dispersion compensated MSF can compensate for the cumulative dispersion of standard single-mode fiber of 18.45 km in the wavelength range of 1385~1575 nm by optimizing MSF parameters. The change range of residual dispersion is within  $\pm 0.72$  ps/(nm·km), and the splicing loss with standard single-mode fiber is controlled below 5 dB within the compensation bandwidth of 190 nm. Compared with the air hole-quartz structure dual-concentric-core microstructure fiber, the designed fiber reduces the difficulty of fiber drawing, is easy to splice with standard single-mode fiber, and has wider compensation bandwidth as well as larger compensation multiple than the existing microstructure fiber. This lays a solid foundation for the optimization of dense wavelength division multiplexing networks and the construction of all-optical networks.

**Keywords:** microstructure fiber; broadband dispersion compensation; all-solid; dual-concentric-core; residual dispersion

## 1. Introduction

Dispersion accumulation has become an inevitable problem in modern ultra-long distance optical fiber communication with ultra-high rate and ultra-wide bandwidth, and it will seriously affect the construction of an all-optical network system. To solve the problem, the cumulative dispersion generated after long distance transmission in all channels needs to be compensated by broadband dispersion compensation (BDC). What's more, the smaller the residual dispersion, the longer the transmission distance of dispersion is limited [1–3].

In 2004, Gerome et al. first proposed that the air hole-quartz structure dual-concentric-core microstructure fiber (DCC-MSF), based on the mode coupling theory, can be used for realizing dispersion compensation of single wavelength [4]. Since then, the air hole-quartz structure DCC-MSF has interested researchers all over the world, and there are now more documents about it [5–7]. In 2016, Partha Sona Maji et al. designed a DCC-MSF. The negative dispersion value varied from  $-1000$  to  $-2500$  ps/(nm·km) within a 200 nm bandwidth. However, the residual dispersion value was not mentioned [8]. The existing problem is that the air hole easily deforms or collapses during the MSF drawing process, which changes the characteristics of MSF. What's more, the collapse of the air hole makes fusing between MSF and single-mode fiber (SMF) more difficult, which greatly limits the industrialization of such MSF in dense wavelength division multiplexing (DWDM) systems. Alternatively, all-solid MSF can be constituted by using the doped rod to replace the air hole. In addition,

a doped rod with a different effective refractive index ( $n_{\text{eff}}$ ) value can be acquired through reasonable doping [9,10].

All-solid MSF has been researched widely in recent years because it has the advantages of low drawing difficulty and can be used for easily accessing existing systems [11,12]. In 2017, Qu et al. presented an all-solid DCC-MSF, which can realize dispersion compensation of single wavelength. Its negative dispersion value at 1550 nm reached  $-32,620$  ps/(nm·km) [13]. However, only compensating the cumulative dispersion of some wavelengths makes it very difficult to satisfy the need of DWDM systems in fiber communication. In 2018, Wang et al. proposed an all-solid DCC-MSF with BDC covering S + C bands. Its compensating multiple was 15.43 times standard SMF, and the residual dispersion value varied within  $\pm 0.15$  ps/(nm·km) [14]. Although the variation range of residual dispersion was small, the compensation multiples and bandwidth were slightly insufficient.

In this paper, an all-solid DCC-MSF with BDC characteristics is presented. The wide-band dispersion compensation in the range of 1385 nm–1575 nm is realized. In addition, it is demonstrated that the designed MSF is easily fabricated and can easily access existing optical network systems, which provides the basis of a theory for new optical transmission medium for the generation of a new DWDM system.

## 2. Numerical Methods and Theories

The MSF with circular air holes arranged in regular array can be simulated by the multi-pole method and CUDOS MOF Utilities software, which can calculate the  $n_{\text{eff}}$ . The dispersion and loss can be obtained through substituting the real and imaginary parts into different equations, respectively [15]. The multi-pole method can also be used to simulate the all-solid MSF.

The basic principle of the multi-pole method is that each component of the electromagnetic field is expressed through Bessel functions in cylindrical coordinates. Then, the Helmholtz equation is solved by using the Maxwell's boundary condition. The waveguide dispersion  $D_w(\lambda)$  is expressed as follows [16]:

$$D_w(\lambda) = -\frac{\lambda}{c} \frac{d^2 \text{Re}[n_{\text{eff}}]}{d\lambda^2} \tag{1}$$

Here,  $c$  is light speed and  $\lambda$  is wavelength.  $\text{Re}[n_{\text{eff}}]$  is the real part of the  $n_{\text{eff}}$  of the fundamental mode.

The total dispersion  $D(\lambda)$  of MSF contains  $D_w(\lambda)$  and the material dispersion  $D_m(\lambda)$ . Their relationship satisfies the following equation [17]:

$$D(\lambda) = D_w(\lambda) + D_m(\lambda) \tag{2}$$

The  $D_m(\lambda)$  can be expressed as [18]:

$$D_m(\lambda) = -\frac{\lambda}{c} \frac{d^2 n_m}{d\lambda^2} \tag{3}$$

Here,  $n_m$  is the  $\text{Re}[n_{\text{eff}}]$  of MSF materials, and can be calculated by the Sellmeier equation. The relationship between dispersion slope (DS) and wavelength is as follows [19]:

$$DS(\lambda) = \frac{dD(\lambda)}{d\lambda} \tag{4}$$

As the wavelength varies, the dispersion, along with DS of MSF, will change. To meet the need of BDC, the dispersion and DS need to be compensated simultaneously. As such, the condition of BDC can be defined as [19]:

$$\begin{cases} D_{\text{SMF}}L_{\text{SMF}} + D_{\text{MSF}}L_{\text{MSF}} = 0 \\ DS_{\text{SMF}}L_{\text{SMF}} + DS_{\text{MSF}}L_{\text{MSF}} = 0 \end{cases} \tag{5}$$

where  $L_{SMF}$ ,  $DS_{SMF}$ , and  $D_{SMF}$  are the length, DS, and dispersion of SMF, respectively.  $L_{MSF}$ ,  $DS_{MSF}$ , and  $D_{MSF}$  is the length, DS, and dispersion of the compensated MSF, respectively. Therefore, the length of compensated MSF needs to satisfy the relationship of  $L_{MSF} = -D_{SMF} * L_{SMF} / D_{MSF}$ . In order to realize BDC, the dispersion and DS of the compensated MSF and SMF should have the relationship of  $D_{MSF} DS_{SMF} = DS_{MSF} D_{SMF}$ . Alongside this, the higher the negative dispersion value of the compensated MSF is, the larger the compensation multiple [19]. Meanwhile, the Kappa (K) value is used to represent the ability of compensating dispersion and DS, expressed as [19]:

$$K = \frac{D(\lambda)}{DS(\lambda)} \tag{6}$$

$K$ 's unit is  $n_m$ . While the  $K$  values of the compensated MSF and SMF are equal, the BDC can be achieved perfectly.

The residual dispersion ( $D_R$ ) can be expressed as [19]:

$$D_R = \frac{D_{SMF} L_{SMF} + D_{MSF} L_{MSF}}{L_{SMF} + L_{MSF}} \tag{7}$$

The mode area ( $A_{eff}$ ) can be expressed as [20]:

$$A_{eff} = \frac{(\int \int_S |E|^2 dx dy)^2}{(\int \int_S |E|^4 dx dy)^2} \tag{8}$$

Here,  $E$  is the propagation amplitude of the transverse electric field in MSF, and  $S$  is the mode field area of MSF. The radius of mode field of MSF,  $\omega_{MSF}$ , should then be gained by the equation  $S = \pi \omega_{MSF}^2$ . The splicing loss ( $L_{splice}$ ) between the compensated MSF and SMF can be expressed as [21]:

$$L_{splice} = -20 \log\left(\frac{2\omega_{SMF}\omega_{MSF}}{\omega_{SMF}^2 + \omega_{MSF}^2}\right) \tag{9}$$

Here,  $\omega_{SMF}$  is the radius of mode field of SMF.

The  $D_{SMF}(\lambda)$  can be calculated through

$$D_{SMF}(\lambda) = \frac{S_0}{4} \left[ \lambda - \frac{\lambda_0^4}{\lambda^3} \right] \tag{10}$$

Here,  $\lambda_0$  is zero-dispersion wavelength of 1311.5 nm and  $S_0$  is zero-dispersion slope of 0.092 ps/nm<sup>2</sup>/km, and  $\lambda$  is wavelength.

The dispersion compensation multiple (DCM) of the designed DCC-MSF to standard SMF can be calculated by

$$DCM = \frac{D_{MSF}(\lambda)}{D_{SMF}(\lambda)} \tag{11}$$

The average dispersion compensation multiple (ADCM) of the designed DCC-MSF to standard SMF can be calculated by

$$ADCM = \frac{DCM_{Max} + DCM_{Min}}{2} \tag{12}$$

### 3. Structural Design and Numerical Analysis

The cross-section and equivalent  $Re[n_{eff}]$  profile of the designed all-solid DCC-MSF is shown in Figure 1. As seen in Figure 1, the MSF is formed by the dielectric cylinder with three different kinds of diameters and  $Re[n_{eff}]$ . The dielectric cylinder possessing the largest diameter and the smallest diameter in the four cladding forms the inner and outer core of MSF, respectively. At present, according

to Handbook of Optical Constants of Solids, by doping fluoride and phosphide into silica properly, the different refractive indices required in this paper can be achieved theoretically. The  $\text{Re}[n_{\text{eff}}]$  of substrate material is  $n_0 = 1.450$ . The  $\text{Re}[n_{\text{eff}}]$  of the dielectric cylinder lying in the inner core, outer core, and the cladding is expressed as  $n_1$ ,  $n_2$ , and  $n_3$ , and the corresponding diameters are defined as  $d_1$ ,  $d_2$ , and  $d_3$ , respectively. Because the inner core region includes the substrate material around the inner core and the inner core material, the equivalent  $\text{Re}[n_{\text{eff}}]$  will be between  $n_0$  and  $n_1$ , as will be the same for the other regions. The space of the adjacent dielectric cylinder is  $\Lambda$ . The primitive parameters of the designed MSF are  $n_1 = 1.465$ ,  $n_2 = 1.380$ ,  $n_3 = 1.320$ ,  $d_1 = 2.2 \mu\text{m}$ ,  $d_2 = 0.51 \mu\text{m}$ ,  $d_3 = 0.8 \mu\text{m}$ , and  $\Lambda = 1.8 \mu\text{m}$ .

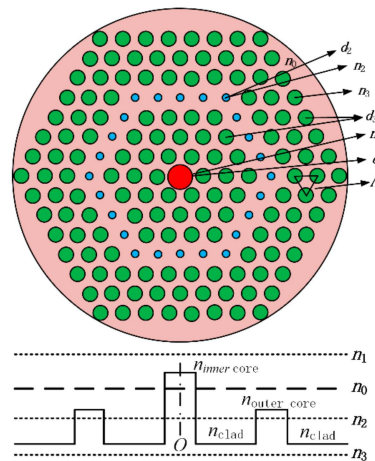


**Figure 1.** Cross-section and equivalent  $\text{Re}[n_{\text{eff}}]$  profile of all-solid dual-concentric-core microstructure fiber (DCC-MSF).

The change of  $\text{Re}[n_{\text{eff}}]$  of the fundamental and second-order supermode is observed in Figure 2a. The illustrations 1, 3 and 2, 4 are the electric field of the fundamental and second-order supermode at different wavelengths, respectively. While smaller than the phase-matching wavelength ( $\lambda_p$ ), the fundamental and second-order supermode transmit in the inner and outer core, separately. There is no energy transferring between the fundamental and second-order supermode. That is to say, the energy of the fundamental and second-order supermode exists in the inner and outer core, respectively. With approaching  $\lambda_p$ , the fundamental and second-order supermode are going to couple. Because of mutating at the intersection of two  $\text{Re}[n_{\text{eff}}]$  curves of the fundamental and second-order supermode, the two modes will generate large negative dispersion and positive dispersion respectively, which is seen in Figure 2b. The positive and negative dispersion reach the maximum value at  $\lambda_p$ . When longer than  $\lambda_p$ , energy transfer will occur. In other words, more and more of the energy of the fundamental supermode transfers from the inner to outer core, and the energy of the second-order supermode goes from the outer to inner core [22,23]. Because the SMF has some positive dispersion in the common communication band, it can be compensated by utilizing the large negative dispersion generated by the fundamental supermode of compensated MSF.

According to the definition of the  $K$  value, BDC is realized perfectly only while the  $K$  value of both the compensated MSF and SMF is equal. Meanwhile, the dispersion and DS are compensated under the circumstances. In terms of Equations (6) and (8), the calculated  $K$  value is shown in Figure 3. The  $K$  value curve of the compensated MSF and SMF exists in the form of a parabolic shape with an upward opening and approximate linear shape, respectively, as seen in Figure 3. The  $K$  value of both the compensated MSF and SMF can't be equal at certain wavelengths under such conditions. However, as the wavelength approaches the point where the  $K$  values are equal, the BDC can be realized approximately due to less variation of the  $K$  value. There are two intersections, at most, of the  $K$  value for both the compensated MSF and SMF, which can be observed in Figure 3. The bandwidth of dispersion compensation realized is wider when there are two intersections in the  $K$  value curve.

What’s more, if either the distance of the two intersections or the difference of the  $K$  values is large, it is difficult to realize BDC. Therefore, in order to realize the BDC, regulating the dispersion and  $K$  value is necessary.

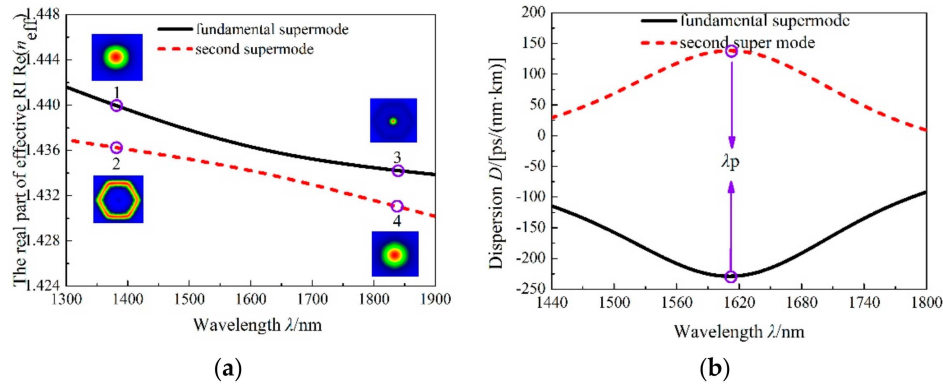


**Figure 2.** Variation of  $\text{Re}(n_{\text{eff}})$  (a) and dispersion (b) with wavelength, the illustration is the mode field distribution of the fundamental and second-order supermode at different wavelengths.

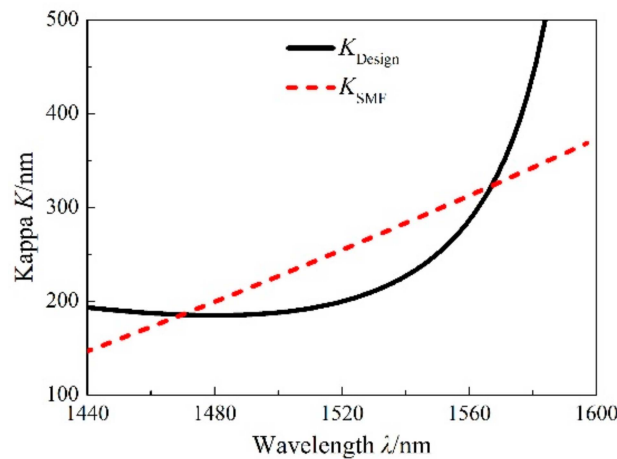


**Figure 3.** Variation of  $K$  value with wavelength.

When the  $\text{Re}[n_{\text{eff}}]$  of the two modes is much closer, coupling can occur more easily. According to the mode coupling theory, this indicates that complete coupling occurs, and the coupling strength is much stronger. The effect of MSF structural parameters on  $\lambda_p$ , dispersion, and the  $K$  value was studied, as shown from Figures 4–7.

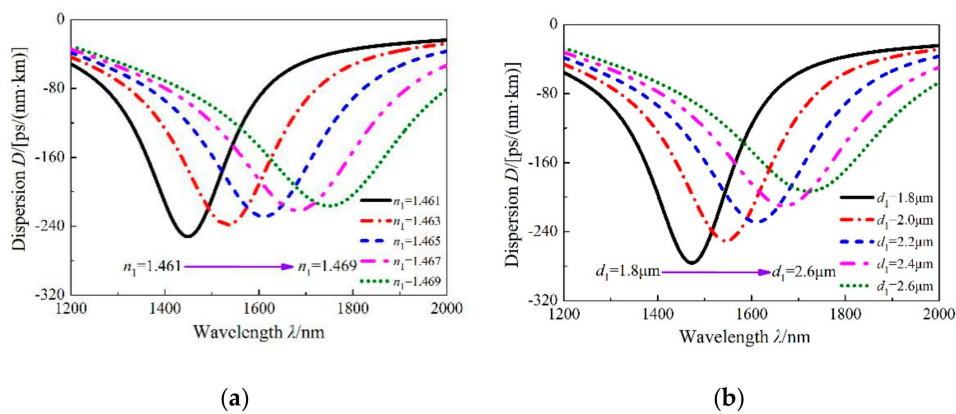


**Figure 4.** Variation of dispersion with  $n_1$  (a) and  $d_1$  (b).

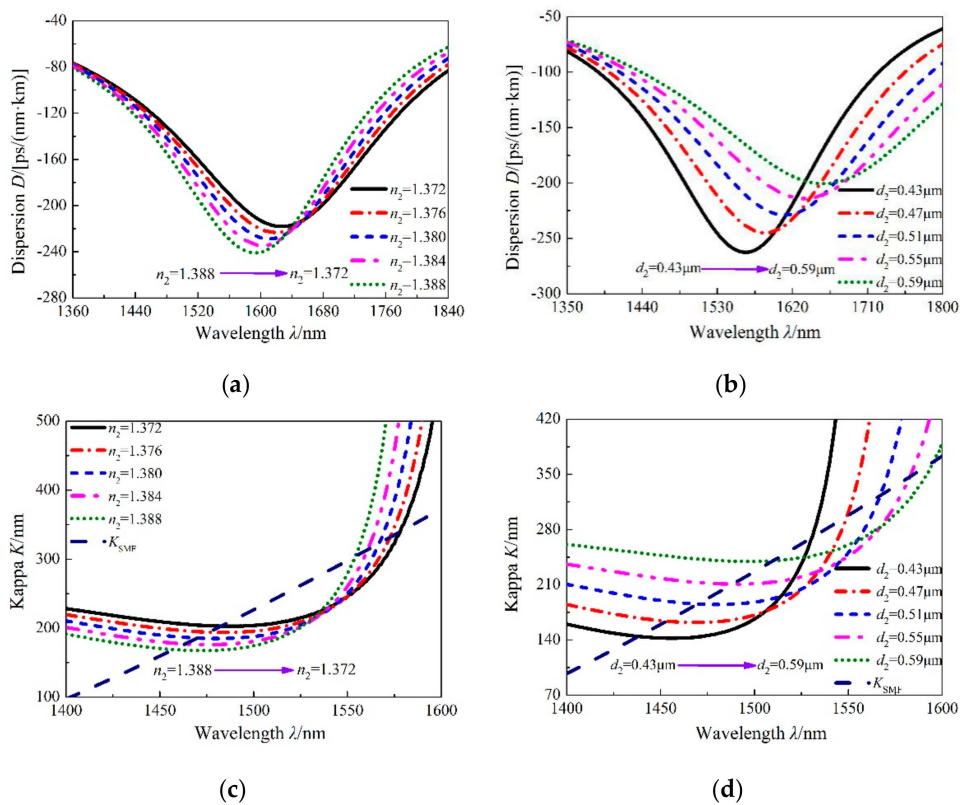


Figure 5. Variation of dispersion (a), (b) and K value (c), (d) with  $n_2$  and  $d_2$ , respectively.

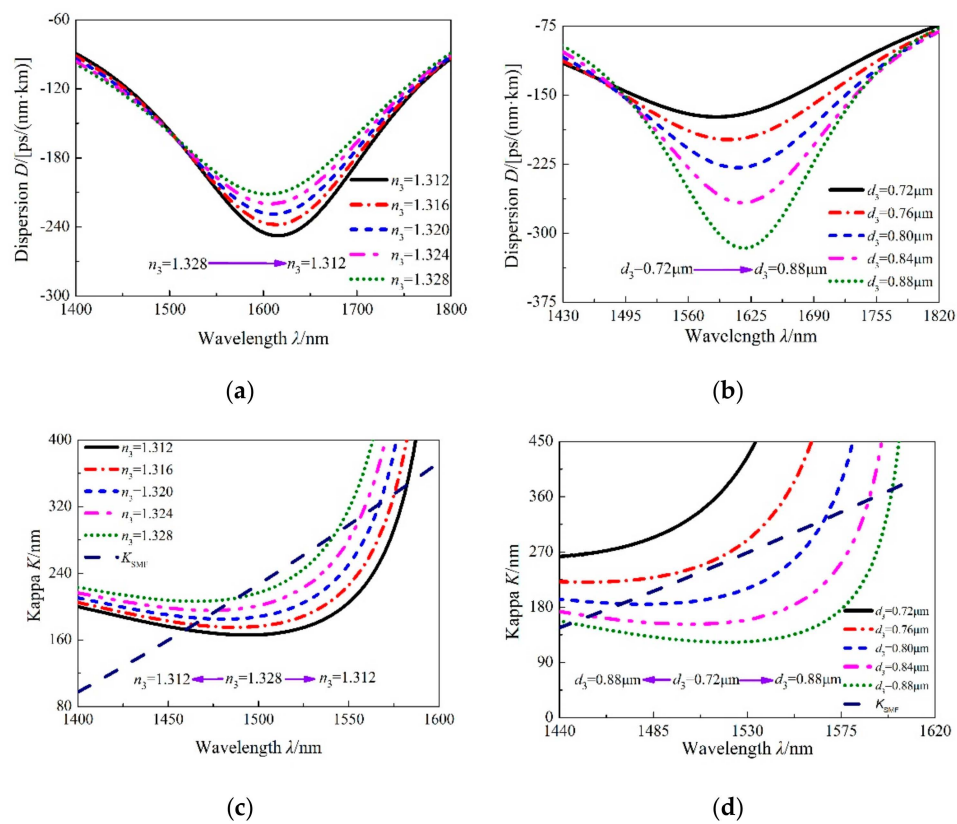


Figure 6. Variation of dispersion (a), (b) and K value (c), (d) with  $n_3$  and  $d_3$ , respectively.

The variation of dispersion with  $n_1$  and  $d_1$  is shown in Figure 4. With  $n_1$  increasing, the  $\text{Re}[n_{\text{eff}}]$  difference between the inner and outer core increases, and  $\lambda_p$  shifts to a longer wavelength. Meanwhile, the negative dispersion value decreases gradually, as observed from Figure 4a. As  $d_1$  becomes bigger,  $\lambda_p$  moves to a longer wavelength. At the same time, the negative dispersion value also decreases gradually, as shown in Figure 4b. Because the variation of  $n_1$  and  $d_1$  has an important impact on  $\lambda_p$  and the negative dispersion value, the  $K$  value changes greatly if the calculation formula of the  $K$  value is adopted under these conditions. This will mean that the condition of BDC is not met, so the variation of the  $K$  value with  $n_1$  and  $d_1$  is not given. In order to obtain a better  $K$  value, the appropriate  $n_1$  and  $d_1$  are chosen first during parameter selection process.

The variations in dispersion and  $K$  values with  $n_2$  and  $d_2$  are shown in Figure 5. As seen from Figure 5a,b, with increasing  $n_2$ , the  $\text{Re}[n_{\text{eff}}]$  difference between the inner and outer core increases, and  $\lambda_p$  shifts to a longer wavelength. At the same time, the negative dispersion value decreases slowly. The increase of  $d_2$  makes  $\lambda_p$  shift to a longer wavelength and the negative dispersion value also decreases gradually. Under the two conditions, the intersection of the  $K$  value of both the compensated MSF and SMF shifts to a longer wavelength, and the  $K$  value increases gradually, as seen in Figure 5c,d. It can be seen that  $n_2$  and  $d_2$  mainly fine-tune negative dispersion and the  $K$  value.

The variation of dispersion and  $K$  value with  $n_3$  and  $d_3$  is shown in Figure 6. When  $n_3$  decreases, the  $\text{Re}[n_{\text{eff}}]$  between the inner and outer core decreases simultaneously, which causes  $\lambda_p$  to have a slight change, and the negative dispersion value to become obviously large, as seen in Figure 6a,b. The increase of  $d_3$  also causes  $\lambda_p$  to have a slight change, and the negative dispersion value to distinctly increase. Under the two conditions, the number of intersections between the  $K$  value curves of both the compensated MSF and SMF varies from zero to two. The intersection is blue-shifted and the  $K$  value gradually decreases at short wavelengths. However, the intersection is red-shifted and the  $K$  value gradually increases at long wavelengths. What's more, the distance between the two intersections is much larger, as seen from Figure 6c,d. Thus, it can be seen that  $n_3$  and  $d_3$  mainly adjust the number of intersection points of the  $K$  values of both the compensated MSF and SMF.

The variation of dispersion and  $K$  values with  $\Lambda$  is shown in Figure 7. As seen from Figure 7a, when  $\Lambda$  increases, the  $\text{Re}[n_{\text{eff}}]$  of the inner and outer core becomes larger, which makes  $\lambda_p$  move to a longer wavelength and the negative dispersion slowly decrease. The two intersections of the  $K$  values of both the compensated MSF and SMF are red-shifted. What's more, the distance of the two intersections is much larger, and the  $K$  value increases gradually at the intersection, which is observed in Figure 7b. It can be seen that  $\Lambda$  mainly roughly adjusts negative dispersion and  $K$  value.

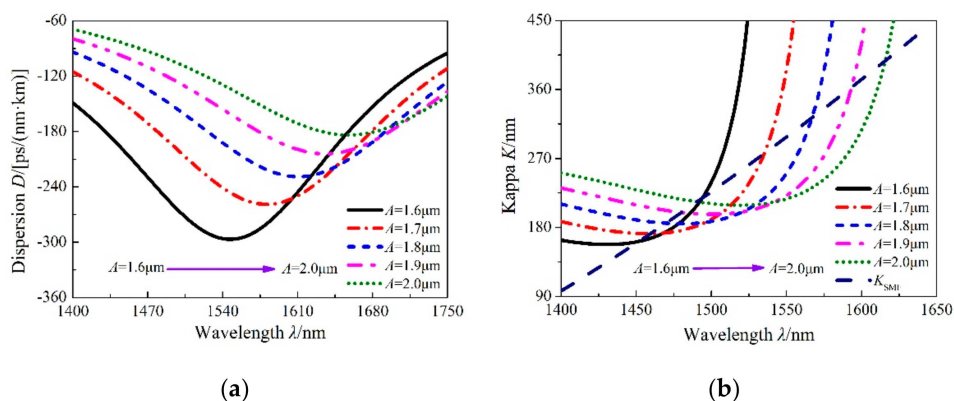
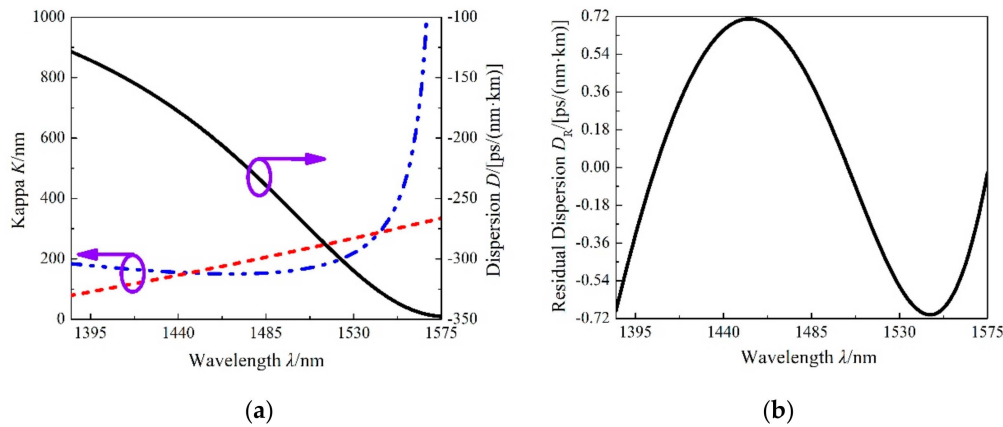


Figure 7. Variation of dispersion (a) and  $K$  value (b) with  $\Lambda$ .

Through optimizing MSF structural parameters, an ultra BDC-MSF with compensation bandwidth of up to 190 nm is proposed when the parameters are  $n_1 = 1.467$ ,  $n_2 = 1.382$ ,  $n_3 = 1.326$ ,  $d_1 = 2.15 \mu\text{m}$ ,  $d_2 = 0.51 \mu\text{m}$ ,  $d_3 = 0.84 \mu\text{m}$ , and  $\Lambda = 1.55 \mu\text{m}$ . From Figure 8a,b, the variation of dispersion,  $K$  value, and residual dispersion after dispersion compensation by using the designed MSF is known.

The ADCM is 18.45 times, and the change range of  $D_R$  is controlled within  $\pm 0.72$  ps/(nm·km) when the wavelength varies from 1385 nm to 1575 nm. As we know, the confinement loss and bend loss of MSF can be controlled effectively by increasing the layer number, therefore the loss curve is not given. The effective mode area of the designed MSF and splice loss with standard SMF are listed in Table 1.



**Figure 8.** Dispersion and  $K$  value (a) as well as  $D_R$  after compensation by using designed microstructure fiber (MSF) (b) with wavelength.

**Table 1.** The effective mode area of designed MSF and splice loss with standard single-mode fiber (SMF).

Wavelength (nm)	1385	1460	1530	1550	1565	1575
$A_{\text{eff}}$ ( $\mu\text{m}^2$ )	6.66	8.15	11.56	13.40	15.21	16.68
$L_{\text{splice}}$ (dB)	4.63	3.95	2.83	2.39	2.06	1.81

According to Equation (9), the parameter affecting the splice loss is the radius of mode field of the fiber, and the radius of mode field is decided by the core diameter of the fiber. Different types of commercially available fibers have different core diameters. However, the core diameter is generally controlled in the range of 8–11  $\mu\text{m}$ . Table 2 shows the splice loss of the designed MSF and commercially available fibers with different core diameters at 1550 nm. From Table 2, there is a low splice loss between the designed MSF and commercially available fibers of different core diameters.

**Table 2.** The splice loss of designed MSF and commercially available SMF with different core diameters at 1550 nm.

Core Diameter ( $\mu\text{m}$ )	8.0	8.5	9.0	9.5	10.0	10.5	11.0
$L_{\text{splice}}$ (dB)	1.77	2.09	2.40	2.72	3.03	3.33	3.63

Table 3 shows the comparison results for compensation bandwidth, ADCM, and  $D_R$  of the proposed and the reported BDC-MSF. From Table 3, the proposed BDC-MSF not only has wider compensation bandwidth and higher compensation multiple, but also has the advantages of low residual dispersion and easy fabrication.

**Table 3.** Comparison with the reported BDC-MSF.

Ref.	Compensation Bandwidth (nm)	ADCM	$D_R$ (ps/(nm·km))	Optical Fiber Structure
[2]	170	17.6	$\pm 1.6$	air hole-quartz DCC structure
[8]	200	Not mentioned	Not mentioned	air hole-quartz DCC structure
[12]	105	15.43	$\pm 0.15$	all-solid DCC structure
This work	190	18.45	$\pm 0.72$	all-solid DCC structure



#### 4. Conclusions

In this paper, an all-solid DCC ultra BDC-MSF is presented. The influence of MSF parameters on  $\lambda_p$ , dispersion, and  $K$  value was studied by making use of the mode coupling mechanism and control variable method. When the parameters are set as  $n_1 = 1.467$ ,  $n_2 = 1.382$ ,  $n_3 = 1.326$ ,  $d_1 = 2.15 \mu\text{m}$ ,  $d_2 = 0.51 \mu\text{m}$ ,  $d_3 = 0.84 \mu\text{m}$ , and  $\Lambda = 1.55 \mu\text{m}$ , the designed MSF has very wide compensation bandwidth of up to 190 nm. The ADCM of the designed BDC-MSF to standard SMF is 18.45 times at 1385~1575 nm. At the same time, the  $D_R$  is within  $\pm 0.72 \text{ ps}/(\text{nm}\cdot\text{km})$ , and the splicing loss with standard SMF can be controlled under 5 dB. What's more, the  $A_{\text{eff}}$  at 1550 nm is  $13.40 \mu\text{m}^2$ . The presented SMF has much wider bandwidth and larger compensation multiple than the literature has previously reported. Compared with the air hole-quartz structure BDC-MSF, the designed MSF reduces the difficulty of fiber drawing and is much easier to fuse with standard SMF. This provides a new basis for the construction of an all-optical network.

**Author Contributions:** C.W. wrote the manuscript, and all authors contributed to the completion of the manuscript.

**Funding:** This research received no external funding.

**Acknowledgments:** Supported by the National Basic Research Program of China (No. 2010CB327604), National Science Foundation of China (Nos. 61405173, 61405172), National Science Foundation of Hebei Province (Nos. F2018105036, F2018203346, F2019105108), Science and Technology Research Project of College and University in Hebei Province (No. BJ2017108), Science and Technology Project of Tangshan City (Nos. 15130263a, 17130257a, 17110220a, 17110221a), PhD Innovation Fund Project of Tangshan University, and Tangshan Key Laboratory of Indoor Location Technology.

**Conflicts of Interest:** The authors declare no conflict of interest.

#### References

1. Gruner-Nielsen, L.; Wandel, M.; Kristensen, P.; Jorgensen, C.; Jorgensen, L.V.; Edvold, B.; Palsdottir, B.; Jakobsen, D. Dispersion-compensating fibers. *J. Lightwave Technol.* **2005**, *23*, 3566–3579. [[CrossRef](#)]
2. Begum, F.; Namihira, Y.; Abdur Razzak, S.M.; Kaijag, S.B.; Hai, N.H.; Kinjo, T.; Miyagi, K.; Zou, N.Y. Novel broadband dispersion compensating photonic crystal fibers: Applications in high-speed transmission systems. *Opt. Laser Technol.* **2009**, *41*, 679–686. [[CrossRef](#)]
3. Matloub, S.; Hosseini, S.M.; Rostami, A. Analysis and optimization of a dual-core dispersion compensation fiber based on a 12-fold photonic quasicrystal structure. *Appl. Opt.* **2014**, *53*, 8366–8373. [[CrossRef](#)] [[PubMed](#)]
4. Gerome, F.; Auguste, J.L.; Blondy, J.M. Design of dispersion-compensating fibres based on a dual-concentric-core photonic crystal fibre. *Opt. Lett.* **2004**, *29*, 2725–2727. [[CrossRef](#)] [[PubMed](#)]
5. Yuan, J.H.; Sang, X.Z.; Yu, C.X.; Jin, C.; Shen, X.W.; Zhou, G.Y.; Li, S.G.; Hou, L.T. Large negative dispersion in dual-concentric-core photonic crystal fiber with hybrid cladding structure based on complete leaky mode coupling. *Opt. Commun.* **2011**, *284*, 5847–5852. [[CrossRef](#)]
6. Zhang, Y.N. Design and optimization of low-loss low-nonlinear high negative-dispersion photonic crystal fibre. *Acta Phys. Sin.* **2012**, *61*, 000261–000267.
7. Hsu, J.M.; Zheng, W.H.; Lee, C.L.; Horng, J.S. Theoretical investigation of a dispersion compensating photonic crystal fibre with ultra-high dispersion coefficient and extremely low confinement loss. *Photonics and Nanostruct.-Fundament. Appl.* **2015**, *16*, 1–8. [[CrossRef](#)]
8. Partha, S.M.; Partha, R.C. ASE suppression in  $\text{Er}^{3+}$  doped dual-core triangular lattice photonic crystal fibers(PCFs) for narrowband and broadband dispersion compensation for communication wavelength. *Optik* **2016**, *127*, 292–298.
9. Poletti, F.; Feng, X.; Ponzio, G.M.; Petrovich, M.N.; Loh, W.H.; Richardson, D.J. All-solid highly nonlinear singlemode fibers with a tailored dispersion profile. *Opt. Express* **2011**, *19*, 66–80. [[CrossRef](#)]
10. Martynkien, T.; Pysz, D.; Stępień, R.; Buczyński, R. All-solid microstructured fiber with flat normal chromatic dispersion. *Opt. Lett.* **2014**, *39*, 2342–2345. [[CrossRef](#)]
11. Granzow, N.; Uebel, P.; Schmidt, M.A.; Tverjanovich, A.S.; Wondraczek, L.; Russell, P.S.J. Bandgap guidance in hybrid chalcogenide-silica photonic crystal fibers. *Opt. Lett.* **2011**, *39*, 2432–2434. [[CrossRef](#)] [[PubMed](#)]
12. Konidakis, I.; Pissadakis, S. Optical spectra tuning of all-glass photonic bandgap fiber infiltrated with silver fast-ion-conducting glasses. *Materials* **2014**, *7*, 5735–5745. [[CrossRef](#)] [[PubMed](#)]

13. Qu, Y.W.; Zhang, C.L.; Guo, C.J.; Zhang, S.; Han, Y.; Zhao, X.T.; Hou, L.T.; Wang, W. Research and design of all-solid dual-concentric-core photonic crystal fiber for dispersion compensation. *Acta Photonica Sin.* **2017**, *46*, 0706005. [[CrossRef](#)]
14. Wang, W.; Qu, Y.W.; Zhang, C.L.; Zuo, Y.T.; Han, Y.; Wang, C.; Qi, Y.F.; Hou, L.T. Novel design of broadband dispersion compensating photonic crystal fiber with all solid structure and low index difference. *Optik* **2018**, *156*, 279–288. [[CrossRef](#)]
15. Fu, B.; Li, S.G.; Yao, Y.Y.; Zhang, L.; Zhang, M.Y. Design of two kinds of dual-core high birefringence and high coupling degree photonic crystal fibers. *Opt. Commun.* **2010**, *283*, 4064–4068. [[CrossRef](#)]
16. Yang, S.G.; Zhang, Y.J.; Peng, X.Z.; Lu, Y.; Xie, S.Z. Theoretical study and experimental fabrication of high negative dispersion photonic crystal fiber with large area mode field. *Opt. Express* **2006**, *14*, 3015–3023. [[CrossRef](#)] [[PubMed](#)]
17. Li, X.Y.; Xu, Z.; Ling, W.; Liu, P. Design of highly nonlinear photonic crystal fibers with flattened chromatic dispersion. *Appl. Opt.* **2014**, *53*, 6682–6687. [[CrossRef](#)] [[PubMed](#)]
18. Hsu, J.M.; Ye, G.S. Dispersion ultrastrong compensating fiber based on a liquid-filled hybrid structure of dual-concentric core and depressed-clad photonic crystal fiber. *J. Opt. Soc. Am. B* **2012**, *29*, 2021–2028. [[CrossRef](#)]
19. Zhao, X.T.; Zhou, G.Y.; Li, S.G.; Liu, Z.L.; Wei, D.B.; Hou, Z.Y.; Hou, L.T. Photonic crystal fiber for dispersion compensation. *Appl. Opt.* **2008**, *47*, 5190–5196. [[CrossRef](#)]
20. De, M.; Gangwar, R.K.; Singh, V.K. Designing of highly birefringence, dispersion shifted decagonal photonic crystal fiber with low confinement loss. *Photonics Nanostruct.-Fundament. Appl.* **2017**, *26*, 15–23. [[CrossRef](#)]
21. Zhou, X.F.; Chen, Z.L.; Chen, H.H.; Hou, J. Fusion splicing small-core photonic crystal fibers and single-mode fibers by controlled air hole collapse. *Opt. Commun.* **2012**, *285*, 5283–5286. [[CrossRef](#)]
22. Zhang, Z.H.; Shi, Y.F.; Bian, B.M.; Lu, J. Dependence of leaky mode coupling on loss in photonic crystal fiber with hybrid cladding. *Opt. Express* **2008**, *16*, 1915–1922. [[CrossRef](#)] [[PubMed](#)]
23. Zhang, Z.H.; Shi, Y.F.; Bian, B.M.; Lu, J. Large negative dispersion in dual-core photonic crystal fibers based on optional mode coupling. *IEEE Photonics Technol. Lett.* **2008**, *20*, 1402–1404. [[CrossRef](#)]



© 2019 by the authors. Licensee MDPI, Basel, Switzerland. This article is an open access article distributed under the terms and conditions of the Creative Commons Attribution (CC BY) license (<http://creativecommons.org/licenses/by/4.0/>).